Journal of Colloid and Interface Science 495 (2017) 207–215

Contents lists available at ScienceDirect

Journal of Colloid and Interface Science

journal homepage: www.elsevier.com/locate/jcis

Regular Article

Acetone gas sensor based on NiO/ZnO hollow spheres: Fast response and recovery, and low (ppb) detection limit

Chang Liu [a,b], Liupeng Zhao [b], Boqun Wang [b], Peng Sun [a,b,*], Qingji Wang [c], Yuan Gao [b], Xishuang Liang [b], Tong Zhang [b], Geyu Lu [a,b,*]

[a] State Key Laboratory of Automotive Simulation and Control, Jilin University, 5988 Renmin Street, Changchun 130012, People's Republic of China
[b] State Key Laboratory on Integrated Optoelectronics, College of Electronic Science and Engineering, Jilin University, 2699 Qianjin Street, Changchun 130012, People's Republic of China
[c] College of Instrumentation and Electrical Engineering, Jilin University, Changchun 130061, People's Republic of China

GRAPHICAL ABSTRACT

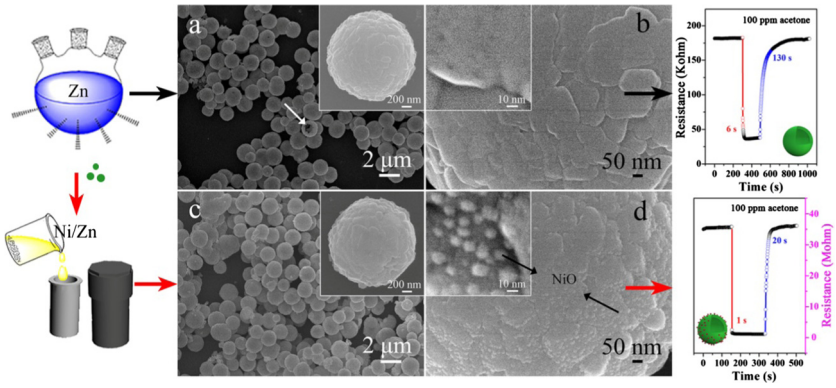

ARTICLE INFO

Article history:
Received 14 November 2016
Revised 25 January 2017
Accepted 26 January 2017
Available online 31 January 2017

Keywords:
NiO/ZnO composites
Hollow spheres
p-n heterostructure
Fast response/recovery
Acetone

ABSTRACT

NiO/ZnO composites were synthesized by decorating numerous NiO nanoparticles on the surfaces of well dispersed ZnO hollow spheres using a facile solvothermal method. Various kinds of characterization methods were utilized to investigate the structures and morphologies of the hybrid materials. The results revealed that the NiO nanoparticles with a size of ~10 nm were successfully distributed on the surfaces of ZnO hollow spheres in a discrete manner. As expected, the NiO/ZnO composites demonstrated dramatic improvements in sensing performances compared with pure ZnO hollow spheres. For example, the response of NiO/ZnO composites to 100 ppm acetone was ~29.8, which was nearly 4.6 times higher than that of primary ZnO at 275 °C, and the response/recovery time were 1/20 s, respectively. Meanwhile, the detection limit could extend down to ppb level. The likely reason for the improved gas sensing properties was also proposed.

1. Introduction

On the basis upon the dramatic merits of high sensitivity, low cost and power consumption, as well as facile integration, gas sensors based on oxide semiconductors have been paid great attention and regarded as one of the effective approaches in the detection of

* Corresponding authors at: State Key Laboratory of Automotive Simulation and Control, Jilin University, 5988 Renmin Street, Changchun 130012, People's Republic of China; State Key Laboratory on Integrated Optoelectronics, College of Electronic Science and Engineering, Jilin University, 2699 Qianjin Street, Changchun 130012, People's Republic of China.
E-mail addresses: pengsun@jlu.edu.cn (P. Sun), lugy@jlu.edu.cn (G. Lu).

http://dx.doi.org/10.1016/j.jcis.2017.01.106
0021-9797/

various harmful, explosive, and toxic gases [1,2]. Over the past few decades, various kinds of metal oxide semiconductors such as (n-type) SnO_2 [3,4], ZnO [5,6], α-Fe_2O_3 [7,8], In_2O_3 [9,10] and (p-type) NiO [11,12], Co_3O_4 [13], CuO [14] have been successfully prepared and widely used in gas sensors. It is clearly acknowledged that the sensing materials play essential roles in determining the sensing performances of sensors. In this regard, great efforts have been made to enhance the sensing properties of traditional metal oxide semiconductors, such as novel metal loading, aliovalent ion doping, as well as the formation of nanocomposites constructed with different semiconductor oxides. Recently, many research results have indicated that oxide semiconductor composites show more superior sensing properties than those of single oxide semiconductors. So far, composites consisting of two or more metal oxides, such as (n-n type) SnO_2/α-Fe_2O_3 [15,16], SnO_2/ZnO [17,43] and (n-p type) NiO/SnO_2 [18,19], CuO/ZnO [20] have been successfully prepared and have improved the sensing properties actually. Despite many satisfying results regarding sensing properties of semiconductor composites have been obtained, compared with that of noble metal catalyst-decorated or transition metal-doped semiconductor-based gas sensors, the sensing mechanism of heterostructure semiconductor composites-based gas sensors is not well established and still in an early stage. Therefore, in order to make continual improvement in gas sensing properties, the investigation of heterostructure composites is of vital scientific and practical significance, and also deserves more efforts.

ZnO, as an important n-type semiconductor oxide with a band gap of ~3.3 eV, has been extensively investigated as a kind of sensing material because of their many merits including relatively high sensitivity, ease of fabrication and low cost [21–24]. However, it also has some unnegligible demerits, such as high operating temperature and poor selectivity [25,26]. Recently, many reported literatures have demonstrated that the acetone-sensing performances of ZnO could be improved by the heterostructure formation techniques. For example, Zhou and co-workers have fabricated gas sensors using ZnO/$ZnCo_2O_4$ hollow spheres synthesized by a facile solvothermal method, demonstrating fast response kinetics to acetone gas [27]. Wang et al. have synthesized $ZnFe_2O_4$/ZnO microstructures through a glucose-assisted hydrothermal method, and the composites showed enhanced acetone properties compared with the pure ZnO [28]. In our previous research, for the first time, the acetone-sensing characteristics of NiO-functionalized ZnO microflowers were experimentally investigated as a function of the surface coverage of NiO nanoparticles [42]. Though some improvements had been obtained, there still existed many shortcomings, such as the detection limit of acetone did not reach the ppb magnitude required for the diagnosis of diabetes [44,45]. In addition, there was still considerable room for improvement in the time of response/recovery. Therefore, it is necessary to further ameliorate the properties of materials for advanced applications. It has been reported that the microstructure, morphology, size, and component of semiconductor oxides exert a significant impact on their sensing properties [46]. Semiconductor oxides with hollow nanostructures have been regarded as promising sensing materials, because this microstructure is beneficial for diffusion of gas, leading to fast response/recovery speed [30]. In this regard, highly uniform ZnO hollow spheres were chosen as the substrates for supporting NiO nanoparticles to utilize their advantages of hollow nature. Meanwhile, since the solution approaches have proven to be among the most effective route to finely tailor semiconductor composites with varying compositional and architectural complexity [48], the solution method was adopted to deposit discrete NiO nanoparticles with smaller size on the surface of ZnO rather than the reported process which sometimes leaded to the agglomeration of NiO nanoparticles and reduced the sensing performance [20,49]. In conclusion, a new strategy was taken to optimize the morphologies of NiO/ZnO composites so as to further investigate the sensing mechanism of p-n metal oxide composites and obtain superior gas sensing properties eventually.

In the present work, we successfully prepared hollow NiO/ZnO composites by combining a microwave-assisted hydrolytic reaction (for the ZnO hollow spheres) and a solvothermal route (for the NiO nanoparticles). As expected, the well-dispersed NiO/ZnO composites demonstrated a great enhancement than those of the ZnO individual component, and showed fast response kinetics and low detection limit to acetone. Additionally, the NiO/ZnO hollow spheres also manifested superior acetone-sensing properties to those reported modified ZnO-based sensors, which are listed in Table 1. The possible origin of the enhanced gas sensing characteristics based on NiO/ZnO composites was discussed.

2. Experimental section

All the reagents in the experiment were analytical-grade purity (Beijing Chemicals Co. Ltd.) and used as received without any further purification.

2.1. Preparation of ZnO hollow spheres

The ZnO hollow spheres were successfully synthesized through a simple liquid-phase reaction with the aid of microwave heating according to the previous literature with some modifications [29]. Generally, 1.10 g of zinc acetate dihydrate ($Zn(CH_3COO)_2{\cdot}2H_2O$) and 0.06 g of trisodium citrate dihydrate ($Na_3C_6H_5O_7{\cdot}2H_2O$) were dissolved into 200 mL deionized water under vigorous stirring. Then, 5 mL of ammonia (30 wt.% NH_3 in water) was added into the above solution drop by drop. After several minutes of fully mixing, the resulting homogeneous solution was transferred into a three-necked flask and maintained at 90 °C for 40 min in a microwave device (MAS-II, Shanghai Xinyi Ltd.), of which the power was set to 300 W. After the reaction, the products were collected by centrifugation, washed with deionized water and ethanol several times, and then dried at 80 °C for 12 h. Finally, the ZnO hollow spheres were obtained by annealing above precipitates at 500 °C for 2 h in a muffle furnace.

2.2. Preparation of NiO/ZnO composites

In a typical procedure, 20 mg of Nickel (II) nitrate hexahydrate ($Ni(NO_3)_2{\cdot}6H_2O$) was first dissolved into a mixed solvent containing 7 mL of ethanol and 3 mL of ethylene glycol under continuous magnetic stirring until a clear solution was achieved. Subsequently, 50 mg of the pre-synthesized ZnO hollow spheres was added into the homogeneous solution by ultrasonic dispersing, and stirred for 20 min. Soon after, the suspension was transferred to a Teflon-lined stainless steel autoclave, which was sealed, kept at 160 °C for 8 h, and then cooled to room temperature naturally. The resulting product was collected via centrifugation and washed with deionized water and ethanol several times, and dried at 80 °C. Eventually, the hollow NiO/ZnO composites were harvested after calcining at 500 °C for 2 h in air. The Ni/Zn ratio of the obtained NiO/ZnO composites was determined to be 2.25 at.%, by inductively coupled plasma mass spectroscopy.

2.3. Characterization

X-ray diffraction (XRD) patterns were recorded using a Rigaku TTRIII X-ray diffractometer with high-intensity Cu Kα radiation (λ = 1.5406 Å) at a scan rate of 4 °/min ranging from 20° to 80° in step of 0.02°, in order to examine the crystal structures of the samples. The morphologies of the products were observed using a

Table 1
Comparison of the acetone-sensing characteristics between a range of modified ZnO-based sensors.

Materials	Temperature (°C)	Concentration (ppm)	Response (R_a/R_g)	Res./Rec. time (s)	Det. lim. (ppm)	Reference
Sn-doped ZnO nanorods	300	200	6.3	7/32	5	[24]
$ZnO/ZnCo_2O_4$ hollow spheres	275	100	7.5	4/36	10	[27]
$ZnFe_2O_4$/ZnO microstructures	320	50	10	13/17	10	[28]
NiO/ZnO microflowers	300	100	23.5	3/41	10	[42]
NiO/ZnO hollow spheres	275	100	30	1/20	0.8	This work

field-emission scanning electron microscope (FESEM, JEOL JSM-7500F, operated at an accelerating voltage of 15 kV). Transmission electron microscopy (TEM) and high-resolution TEM images were acquired to investigate both the morphological and crystalline features of as-prepared samples from a JEM-2200FS (JEOL) transmission electron microscope with an operating voltage of 200 kV. The energy-dispersive X-ray spectrometry (EDS) was applied to study the chemical compositions of the products, which were performed by the TEM attachment. The X-ray photoelectron spectroscopy (XPS) measurements were provided with Mg Kα Xray source (1253.6 eV Specs XR50) at room temperature. Element analysis was carried out on a PerkinElmer Optima 3300 DV Inductively coupled plasma mass spectrometry (ICP-MS) instrument.

2.4. Fabrication and measurement of gas sensor

For comparison, two gas sensors based on pristine ZnO and NiO nanoparticles-decorated ZnO hollow spheres were fabricated, respectively. Taking the sensor using pristine ZnO hollow spheres as an example, the process used to fabricate the gas sensors can be described as follows. An appropriate amount of the as-prepared ZnO hollow spheres was mixed with deionized water to form a homogeneous paste, and then the paste was coated onto the outside surface of a ceramic tube by a paint pen, on which a pair of Au electrodes was installed at each end connected by Pt wires, to form a sensing film. Subsequently, the resulting sensing device was calcined at 400 °C for 2 h to enhance its stability for the measurement of sensing performances. Finally, a Ni-Cr alloy coil was inserted into the tube as a heater to ensure the operating temperature can be controlled by adjusting the heating current flowing through the heater.

The gas sensing characters were investigated by a static gas sensing characterization system under laboratory conditions (30% relative humidity, 20 °C). At the beginning, the sensor was put into a chamber, which was full of fresh air, and then a given amount of test gases was injected into the chamber with the aid of a microsyringe. After that, the sensor was put into the chamber to react with the target gas molecules. When the resistance reached the final equilibrium value, the sensor was transferred into another chamber that was full of fresh air and began to recover. The gas response was defined as $S = R_a/R_g$ for reducing gas, where R_a and R_g are the resistances measured in air and the tested gas atmosphere, respectively. The time consumed by the sensor to reach 90% of the total resistance change in tested gases and fresh air were defined as the response time and recovery time, respectively.

3. Results and discussion

3.1. Structural and morphological characteristics

XRD analysis associated with pure ZnO and NiO/ZnO composites was performed to investigate the crystal structure and purity of the as-synthesized samples, which is displayed in Fig. 1. Obviously, all the diffraction peaks for pure ZnO (shown in Fig. 1a) matched well with those of standard XRD patterns of the hexagonal wurtzite structure of ZnO with lattice constants of a = 3.249 Å and c = 5.206 Å, which agreed well with the reported values from the standard JCPDS Card No. 36-1451. In the meantime, the crystal phases of the composites were clearly shown in Fig. 1b. Most of the diffraction peaks could be indexed to the hexagonal wurtzite structure of ZnO and the residual peak at $2\theta = 43.25°$ could be probably assigned to the cubic structure of NiO with space group *Fm*-3*m* (No. 225) and lattice parameter of a = 4.18 Å, which were consistent with those from the standard data file card No. 73-1523. As a result, the composites were confirmed as mixed oxide of ZnO and NiO. The smaller reflection peaks for NiO than those for ZnO might be due to the smaller volume of the well-dispersed NiO nanoparticles than those of ZnO hollow spheres. No other diffraction peaks corresponding to impurities could be detected, indicating the high purity of the samples.

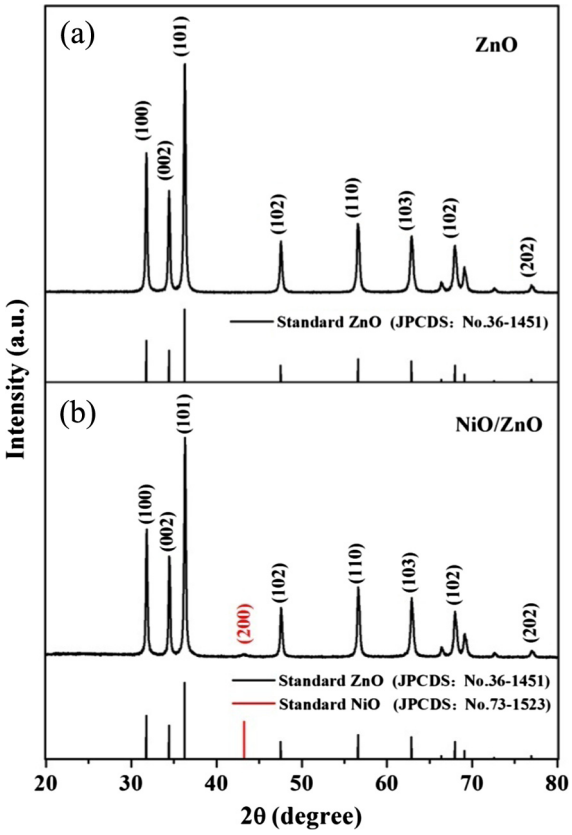

Fig. 1. XRD patterns of the as-prepared products (a) pure ZnO and (b) NiO/ZnO composites.

The size and morphology of the as-prepared pure ZnO and NiO-modified ZnO were observed by FESEM, as shown in Fig. 2. A panoramic FESEM image of the as-prepared pristine ZnO is presented in Fig. 2a, from which a number of monodisperse spheres with a diameter of ~1.5 μm could be clearly observed. Moreover, a broken structure near the center of the image indicated that the spherical architectures were probably hollow. Further observing in the high-magnification FESEM image of Fig. 2b confirmed

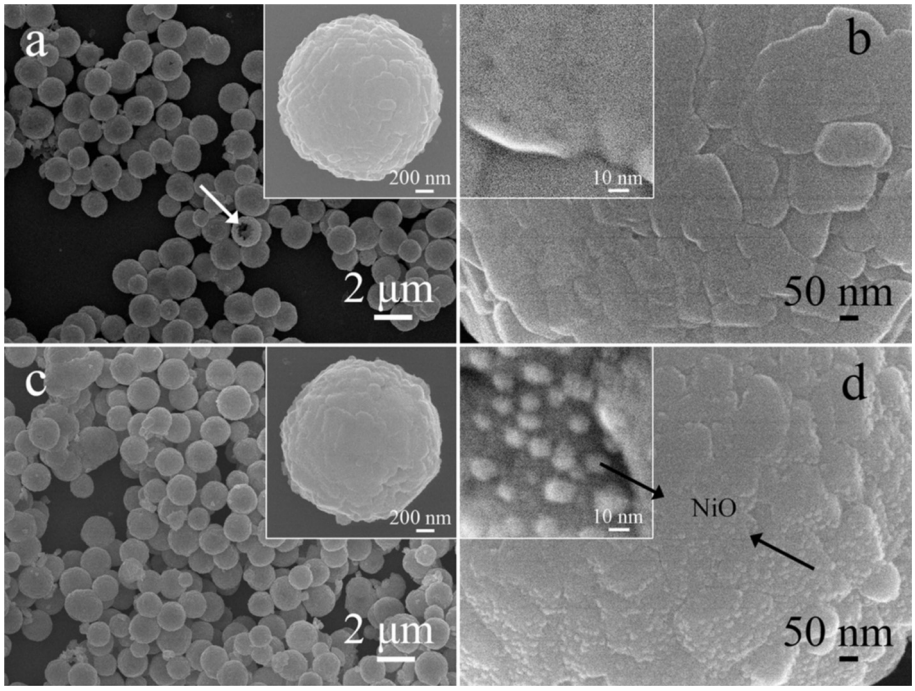

Fig. 2. FESEM images of the as-obtained products, (a) and (b) primary ZnO hollow spheres, (c) and (d) NiO/ZnO composites.

that the surfaces of naked ZnO were relatively smooth. Fig. 2c shows a typical low-magnification FESEM image of the composites, where NiO/ZnO composites were found somewhat similar with pristine ZnO in appearance. Apparently, no other morphologies could be observed, indicating the ideal yield of the products. When a detailed observation in Fig. 2d was taken, it was explicitly demonstrated that the surfaces of NiO/ZnO composites were quite different, and turned coarser compared with those of pristine ZnO hollow spheres. The discrete particles with a size of ~10 nm were likely to be the NiO nanoparticles which had been successfully decorated onto the pristine ZnO substrates (inset of Fig. 2d). Besides, it was worthwhile noting that such hollow structures with rough surfaces endowed the NiO/ZnO composites a high surface area and abundant active sites, which would facilitate the gas diffusion towards the entire sensing materials and an improvement of the sensing properties [30].

TEM and HRTEM were employed to further investigate the as-prepared samples. The typical TEM image (Fig. 3a) of an individual ZnO hollow sphere shows that both the size and morphology were similar to the observations of FESEM, and the hollow nature got further confirmed by the strong contrast between the light center and the dark fringe. The diffraction spots in the SAED pattern suggest that the basic structural unit of ZnO hollow spheres was a single crystal, as shown in the inset of Fig. 3a. According to Fig. 3b, the lattice fringes could be clearly observed and the lattice spacing was 0.281 nm, corresponding to the (100) planes of ZnO. In order to get a deep insight into the NiO/ZnO composites, TEM and HRTEM images were also taken as revealed in Fig. 3c and d. It was clearly seen that all of the spheres possessed a hollow cavity inside (Fig. 3c). Different from the bare ZnO, the surfaces of the NiO/ZnO composites were coated with discrete nanoparticles as shown in Fig. 3d, which was in good accordance with the FESEM observations. Furthermore, the lattice fringes of 0.281 nm and 0.241 nm were assigned to the (100) plane of wurtzite ZnO and the (111) plane of cubic NiO, corresponding to the marked white region and red region, respectively. Thus, the conclusion could be made undoubtedly that the NiO nanoparticles indeed adhered to the surfaces of ZnO with a discrete but not continuous configuration. Afterwards, EDS elemental mapping analysis corresponding to an individual NiO/ZnO hollow sphere (Fig. 3e) further confirmed the spatial distributions of Zn and Ni elements (Fig. 3f and g). Obviously, Zn and Ni signals were detected as a spherical structure, while Ni signals were detected in the whole region, which indicated the uniform distributions of NiO nanoparticles over the entire surfaces of ZnO hollow architectures.

3.2. Gas sensing characteristics

In order to demonstrate the potential application in gas detection, gas sensors made of pure ZnO and NiO nanoparticles-decorated ZnO hollow spheres were fabricated and their gas sensing properties were investigated based on the related experiment, respectively.

First of all, considering that the sensing performances of sensor devices based on metal oxide semiconductors are largely dependent on the operating temperature, the temperature dependent features of the as-fabricated sensors were measured at a wide temperature range to explore the relationship between operating temperature and the gas response, as summarized in Fig. 4a. It shows the response value of the two kinds of sensors to 100 ppm acetone as a function of the operating temperature, from which the volcano-shaped correlation between gas response and operating temperature was observed for both of the two kinds of sensors. In terms of the sensor based on NiO/ZnO composites, when the operating temperature was below 275 °C, the gas molecules didn't have enough thermal energy to make full reaction with oxygen species. As a result, the value of response was relatively low. However, with the increase of the operating temperature above 275 °C, the gas molecules were easy to desorption, leading to the low utilization rate of the sensing material [31,32]. Therefore, 275 °C was chosen as the optimal operating temperature for NiO/ZnO composites-based sensor, at which the oxidation rate of acetone molecules was maximized. Similar behavior could be observed in the case of pure ZnO-based sensor. Noticeably, for pure ZnO, the

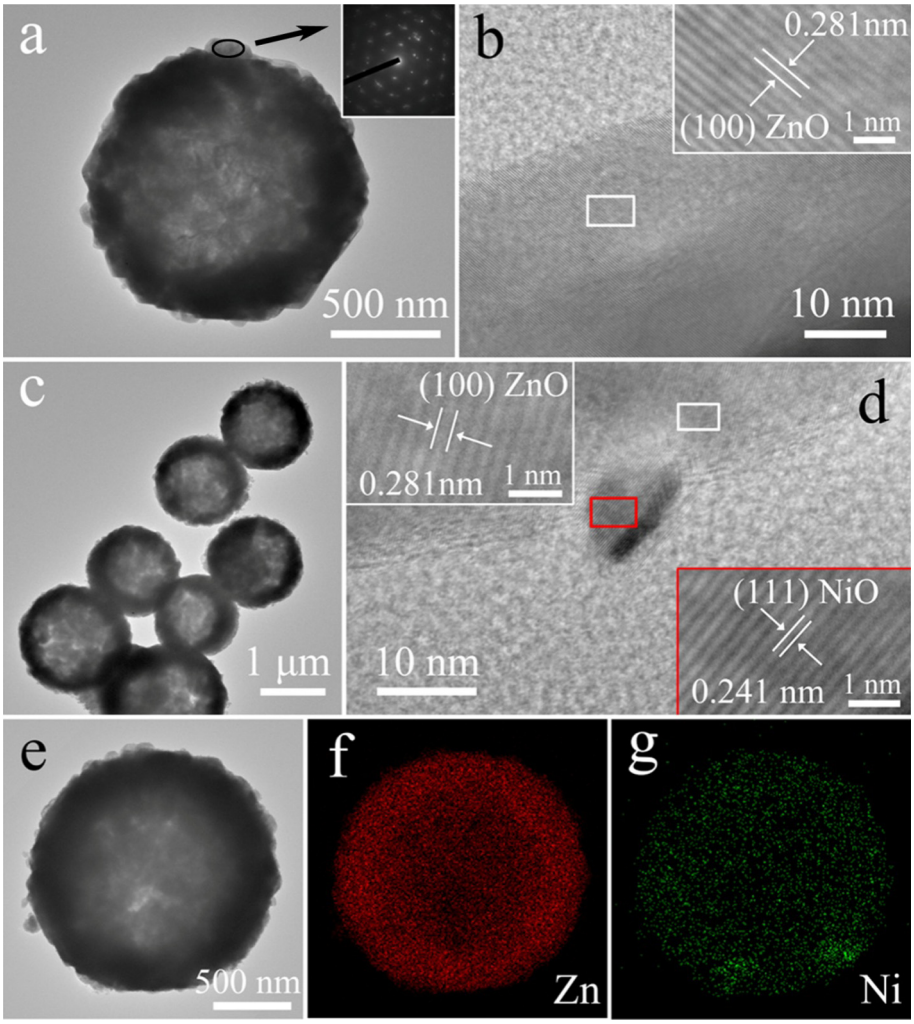

Fig. 3. (a) TEM image of an individual ZnO hollow sphere. (b) The corresponding HRTEM image. (c) TEM image of NiO/ZnO hollow spheres. (d) The corresponding HRTEM image. (e–g) TEM image of an individual NiO/ZnO hollow sphere and the corresponding elemental mapping images.

maximum response was ~9.2 at 325 °C. In contrast, the NiO/ZnO composites exhibited a desirable value of ~29.8 along with a lower temperature of 275 °C, which was as 3.2-fold high as pure ZnO hollow spheres at their optimal operating temperature, respectively.

Subsequently, a response comparison between the sensors based on pure ZnO and NiO/ZnO composites towards a variety of volatile organic gases, such as acetone, methanol, ethanol, etc., was carried out and the results are explicitly shown in Fig. 4b. All of the gases were tested at an operating temperature of 275 °C with a concentration of 100 ppm. It was obvious that the sensor based on NiO/ZnO composites displayed an enhanced response for each target gas when compared with pure ZnO-based sensor. Especially, the sensor using NiO/ZnO composites manifested the highest response to acetone with the value of 1.0–10.2 times higher than other target gases, while ratio was only 0.3–3.6 for the primary ZnO. Consequently, the modification of ZnO hollow spheres with discrete NiO nanoparticles significantly improved the selectivity towards acetone at the same conditions.

Fig. 5a depicts the continuous real-time response and recovery curves of the sensors based on pure ZnO and the NiO/ZnO composites upon exposure to acetone with increasing concentrations ranging from 800 ppb to 100 ppm at 275 °C. Obviously, both of them displayed an excellent response and recovery characteristic, but the response value of the sensor based on NiO/ZnO composites increased much faster and showed an enhanced response at each concentration of acetone. Surprisingly, the lowest acetone detection limit of the NiO/ZnO composites-based sensor was estimated to be <1 ppm (S = 1.6, 800 ppb), with $R_a/R_g > 1.2$ being used as the criterion for gas detection [33]. In Fig. 5b, a stepwise distribution which described the response values accompanied by the increasing of acetone could be intuitively observed for both sensors. When the concentration of acetone was as high as 800 ppm, the NiO/ZnO composites-based sensor did not tend to be saturate, even though the increasing trend gradually slowed down with the increase of the acetone concentration. The result indicated that the sensor consisting of NiO/ZnO composites showed not only a relatively low detection limit, but also a broad detection range. In addition, it is well-known that the human breath contains about 80–98% relative humidity (RH), so the detection of acetone in the presence of the RH is of great importance. The responses of the NiO/ZnO composites upon exposure to low concentrations of acetone in laboratory conditions (30% RH) and humid air (90% RH) are shown in Fig. 5c. The responses decreased as the RH increased to human breath levels, due to the displacement of chemisorbed oxygen species by water molecules and hydroxyl species which formed are the sensor surface [44]. Nevertheless, when the acetone concentration ranged from 1 to 5 ppm, the responses were about 1.3–2.0, which would meet the requirements for diabetes diagnosis (threshold limit 1.7 ppm) [45].

In order to have a deep insight into the sensing characteristics of the as-fabricated sensors, the dynamic response curves for pure ZnO and NiO/ZnO composites-based sensors towards 100 ppm

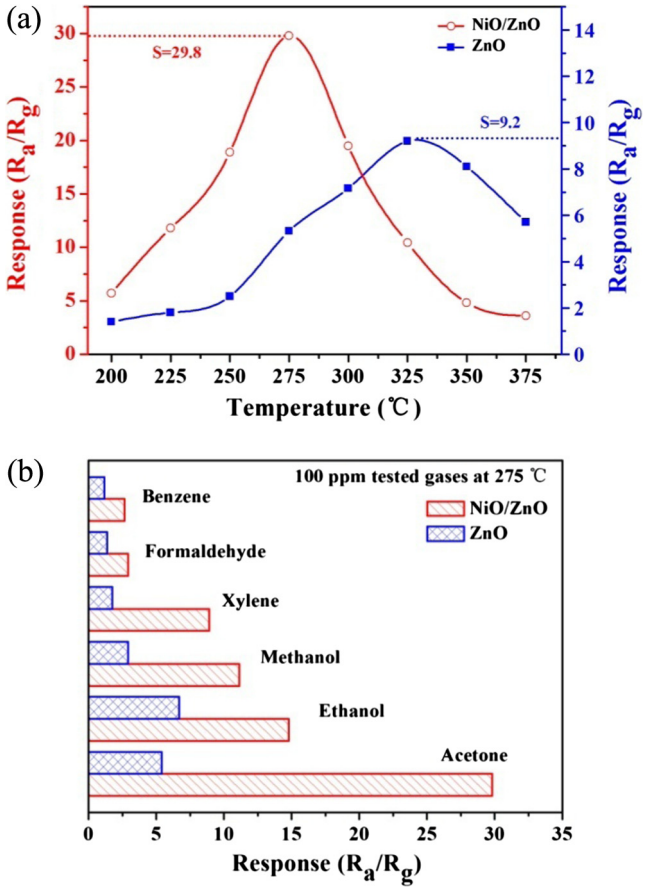

Fig. 4. (a) Responses of the sensors based on the pure ZnO and NiO nanoparticles-decorated ZnO hollow spheres as a function of operating temperature to 100 ppm acetone. (b) Selectivity measurements of the pristine ZnO and NiO/ZnO composites to various tested gases with concentrations of 100 ppm.

acetone at the operating temperature of 275 °C are shown in Fig. 6a and b, respectively. Like pure ZnO displayed in Fig. 6a, there was a decrease and increase in NiO/ZnO composites-based sensor resistance (Fig. 6b) upon exposure to acetone (reducing gas) and air, respectively, which was in good accord with the chemiresistive variation of n-type oxide semiconductors. This indicated that the conduction in NiO nanoparticles-decorated ZnO hollow spheres did not occur along the discrete configuration of p-type NiO but rather through the n-type ZnO and showed that the NiO/ZnO composites was a n-type semiconductor. Furthermore, according to the definition of response/recovery time, the response and recovery

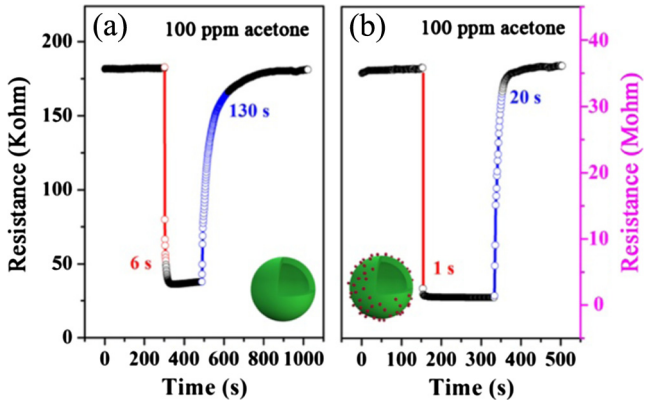

Fig. 6. (a) Response transient of ZnO hollow spheres to acetone with a concentration of 100 ppm at 275 °C. (b) Response transient of NiO/ZnO hollow spheres at the same conditions.

time were only 1 s and 20 s for NiO/ZnO composites, while in terms of the pure ZnO, the time consumed were as long as 6 s and 130 s, respectively. The rapid response and recovery time the NiO/ZnO composites-based sensor demonstrated would make it to be a great candidate for acetone detection.

The long-term stability, as one of the most important criterions for evaluating the performance of gas sensors, was also investigated. The transient sensing responses of sensor based on NiO/ZnO composites to 100 ppm acetone at 275 °C during 16 days are shown in Fig. 7. It was easily noticed that there was little variation in the initial resistance (R_0) in air, which suggested that the NiO/ZnO hollow spheres possessed a strong robustness. In addition, the change amplitude of the responses for fabricated sensor during the tested days was controlled within 11.0%, further verifying the splendid properties of the sensor based on NiO/ZnO composites.

3.3. Gas sensing mechanism

It has been generally acknowledged that the sensing mechanism of n-type semiconducting metal oxides such as the pristine ZnO can be explained in terms of the modulation of depletion layers by oxygen adsorption [34], which may result in the change in resistance of the sensor when exposed to different gas atmospheres. In ambient air, oxygen molecules adsorb on the surfaces of ZnO hollow spheres and ionize to surface-adsorbed oxygen species by capturing free electrons from ZnO, as shown in Eqs. (1) and (2).

$$O_2 + e^- \leftrightarrow O_2^- \quad (1)$$

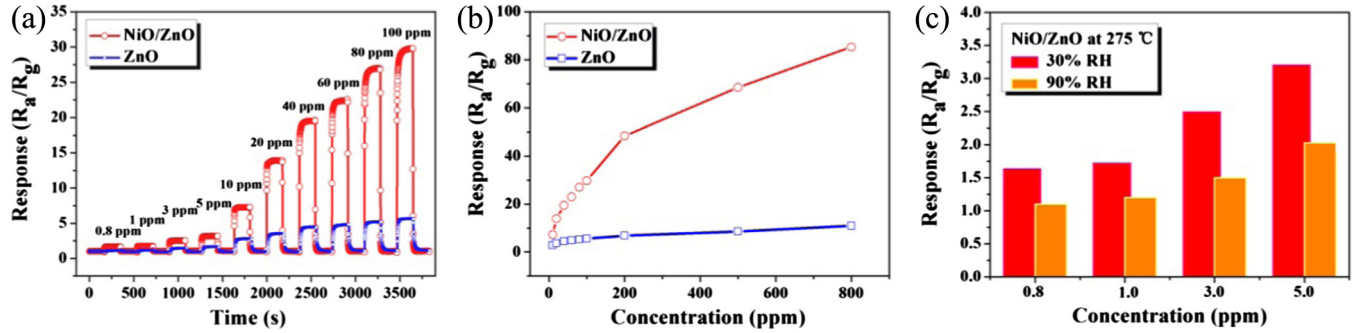

Fig. 5. (a) Dynamic response and recovery curves of pristine ZnO and NiO/ZnO composites to different concentrations of acetone at 275 °C. (b) Responses vs acetone concentration for pure ZnO and NiO/ZnO composites at 275 °C. (c) Responses vs low concentrations of acetone under different relative humidity.

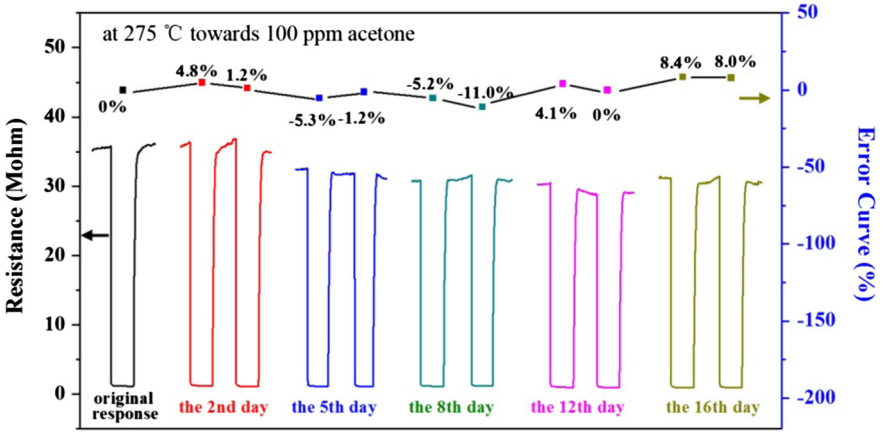

Fig. 7. The dynamic responses of the sensor based on NiO nanoparticles-decorated ZnO hollow spheres upon exposure to 100 ppm acetone at 275 °C during 16 days.

$$O_2^- + e^- \leftrightarrow 2O^- \quad (2)$$

As a result, a thick electron depletion layer forms on the surface region of ZnO, leading to a relative high resistance of the sensor. In the presence of reducing gases, for instance, acetone at a moderate temperature, the acetone molecules react with the former adsorbed oxygen species and make the captured electrons release back to the conduction band of ZnO, which is shown in Eq. (3).

$$CH_3COCH_3 + 8O^- \leftrightarrow 3CO_2 + 3H_2O + 8e^- \quad (3)$$

Thus, the free electron concentration increases and the measured resistance of the sensor decreases finally.

In terms of the sensor based on NiO/ZnO hollow spheres, carriers transport between the n-type ZnO and p-type NiO, which plays a predominant role in the enhanced gas performances. In dry air, because the Fermi level of ZnO is higher than that of NiO [21], electrons will flow from n-type ZnO to p-type NiO while holes will flow along the contrary direction until a balance is obtained (Fig. 8a). Thus, a barrier (p-n junction between n-type ZnO and p-type NiO) will be formed. As a result, the formation of p-n junction causes a high-resistance state in the air. However, in acetone gas, the target gas molecules react with the adsorbed oxygen species, causing electron transfer and changing in electrical conductivity. Essentially, according to the semiconductor theory, the resistance (R) related to heterojunction barrier can be expressed by Eq. (4).

$$R \propto B \exp\left(\frac{q\Phi}{kT}\right) \quad (4)$$

In Eq. (4), B is a constant related to ambient temperature, Φ the heterojunction barrier, k the Boltzmann's constant and T is the absolute temperature. Surface reactions [35,36] result in the decrease in the height of the barrier potential. Consequently, the conductivity of the material will greatly vary even if a very small change occurs in the barrier height, which leads to the strong promotion of sensitivity.

Meanwhile, on the basis of the discrete distribution and the smaller grain size of NiO compared with that of ZnO, it is not difficult to deduce that the conductive paths are mainly along the surfaces of ZnO matrix, which is consistent with the n-type sensing behavior of the composites. Therefore, an additional electron depletion expansion in the ZnO surface should not be neglected when a p-n junction is formed at the same time. In air, a depletion layer and an accumulation layer are formed by the adsorbed oxygen at the exposed surfaces of the ZnO and NiO, respectively. In this case, the electron-transfer reactions will be largely promoted at the interface between ZnO and NiO because of the existence of the accumulation layer on the NiO side which is acknowledged to attach large amounts of the adsorbed oxygen [47]. Thus, an additional electron depletion layer expands in the ZnO surface, which should be taken into account as the other parameter that can significantly affect the measured resistance in air, as evidenced by the phenomenon that the measured value of the resistance was two orders of magnitude higher than that of the pure ZnO-based sensor at the same conditions. While in reducing gas like acetone, the NiO nanoparticles become "less p-type" in such an abundant electrons atmosphere, inducing the strong shrink in the depletion region of ZnO. The process is vividly depicted in Fig. 8b. As a proof-of-concept demonstration of the enhanced amounts of absorbed oxygen in NiO/ZnO composites, the O 1s XPS spectra of the pure ZnO and NiO/ZnO composites were investigated as shown in Fig. 8c and d, respectively. It is widely acknowledged that the peak at ~530.1 eV could be assigned to typical surface lattice oxygen (O_L) and the other peak locating at ~531.6 eV was characteristic of surface absorbed oxygen species (O_C) [37]. For the two kinds of the samples, the relative percentages of the O_C component were about 20.6% (pure ZnO) and 32.6% (NiO/ZnO composites), which provides a strong evidence that the discrete NiO nanoparticles loading on the surfaces of ZnO matrix attracted large amounts of the absorbed oxygen and acted as an electrons-tuning machine during the process of adsorption and desorption of acetone gas. Therefore, a considerable change in the depletion layer in ZnO substrates could be obtained, giving rise to the excellent performances of the NiO/ZnO composites-based sensor.

Apart from the above electronic sensing mechanism, the chemical mechanism related to the high oxidative catalytic activity of NiO towards organic species should also be taken into account because of the decrease in the activation energy of catalytic oxidation caused by NiO [38–40]. Park et al. [41] have reported that the response of sensing material to a certain gas depend on many factors, such as solid solubility of the gas in the material, the decomposition rate of the adsorbed molecule at material surface, the charge carrier concentration in the material, the catalytic activity of the material, and so on. Considering these possible reasons, when compared with the bare ZnO sensor, the sensor based on NiO/ZnO composites exhibited higher response fortunately to acetone may be mainly due to the catalytic discrepancy between the materials and the tested gases, and the higher oxidation rate of acetone on the surface of ZnO and NiO at an appropriate temperature of 275 °C. Spontaneously, the sensor exhibited a rapid response and recovery time when using such hollow architectures in that case. The sensing

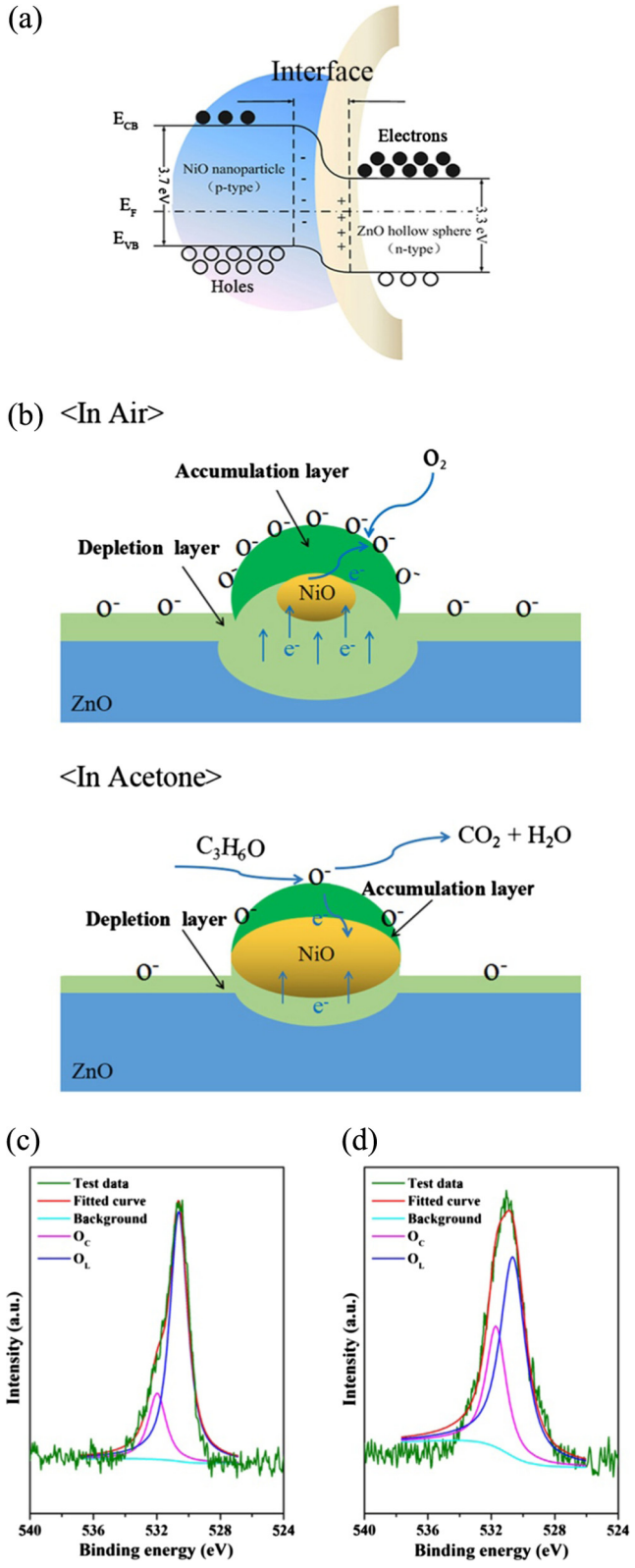

Fig. 8. (a) Energy band diagrams of the NiO/ZnO heterocontact. (b) Schematic diagrams depicting the depletion layer and potential barrier forming at the NiO/ZnO junction upon exposure to air and acetone. (c) O 1s spectra of single-component ZnO hollow spheres. (d) O 1s spectra of the as-prepared NiO/ZnO composites.

performance of the sensor based on NiO nanoparticles-decorated ZnO hollow spheres is believed to be improved by the combination of these reasonable factors.

4. Conclusions

In summary, the uniform NiO nanoparticles-decorated ZnO hollow spheres, prepared by a two-step controllable solution route, were investigated as the high-performance gas sensing materials for detecting acetone. The enhancements of sensitivity, detection limit, as well as the response/recovery speed were achieved by the introduction of NiO nanoparticles loading onto the surfaces of ZnO hollow spheres in a discrete manner. The effect of the p-n junction between NiO and ZnO, the additional extension of electron depletion layer in ZnO matrix, and the catalytic actions of NiO for the oxidation reactions were considered as the key factors to the enhanced gas sensing performances reasonably.

Acknowledgements

This work is supported by the National Nature Science Foundation of China (Nos. 61520106003, 61503148, 61327804, 61374218, 61134010) and Program for Chang Jiang Scholars and Innovative Research Team in University (No. IRT13018). National High-Tech Research and Development Program of China (863 Program, Nos. 2013AA030902 and 2014AA06A505). China Postdoctoral Science Foundation funded project No. 2015M580247.

References

[1] K. Wetchakun, T. Samerjai, N. Tamaekong, C. Liewhiran, C. Siriwong, V. Kruefu, A. Wisitsoraat, A. Tuantranont, S. Phanichphant, Semiconducting metal oxides as sensors for environmentally hazardous gases, Sens. Actuat. B: Chem. 160 (2011) 580–591.
[2] N. Yamazoe, Toward innovations of gas sensor technology, Sens. Actuat. B: Chem. 108 (2005) 2–14.
[3] S. Singkammo, A. Wisitsoraat, C. Sriprachuabwong, A. Tuantranont, S. Phanichphant, C. Liewhiran, Electrolytically exfoliated graphene-loaded flame-made Ni-doped SnO_2 composite film for acetone sensing, ACS Appl. Mater. Interf. 7 (2015) 3077–3092.
[4] D.J. Yang, I. Kamienchick, D.Y. Youn, A. Rothschild, I.D. Kim, Ultrasensitive and highly selective gas sensors based on electrospun SnO_2 nanofibers modified by Pd loading, Adv. Funct. Mater. 20 (2010) 4258–4264.
[5] A. Katoch, Z.U. Abideen, J.-H. Kim, S.S. Kim, Influence of hollowness variation on the gas-sensing properties of ZnO hollow nanofibers, Sens. Actuat. B: Chem. 232 (2016) 698–704.
[6] M.R. Alenezi, S.J. Henley, N.G. Emerson, S.R.P. Silva, From 1D and 2D ZnO nanostructures to 3D hierarchical structures with enhanced gas sensing properties, Nanoscale 6 (2014) 235–247.
[7] H.J. Song, X.H. Jia, H. Qi, X.F. Yang, H. Tang, C.Y. Min, Flexible morphology-controlled synthesis of monodisperse α-Fe_2O_3 hierarchical hollow microspheres and their gas-sensing properties, J. Mater. Chem. 22 (2012) 3508–3516.
[8] H.-J. Kim, K.-I. Choi, A.Q. Pan, I.-D. Kim, H.-R. Kim, K.-M. Kim, C.W. Na, G.Z. Cao, J.-H. Lee, Template-free solvothermal synthesis of hollow hematite spheres and their applications in gas sensors and Li-ion batteries, J. Mater. Chem. 21 (2011) 6549–6555.
[9] S.-J. Kim, I.-S. Hwang, C.-W. Na, I.-D. Kim, Y.C. Kang, J.-H. Lee, Ultrasensitive and selective C_2H_5OH sensors using Rh-loaded In_2O_3 hollow spheres, J. Mater. Chem. 21 (2011) 18477–18488.
[10] T. Waitz, T. Wagner, T. Sauerwald, C.-D. Kohl, M. Tiemann, Ordered mesoporous In_2O_3: synthesis by structure replication and application as a methane gas sensor, Adv. Funct. Mater. 19 (2009) 653–661.
[11] G.H. Li, X.W. Wang, L. Liu, R. Liu, F.P. Shen, Z. Cui, C. Wang, T. Zhang, Controllable synthesis of 3D $Ni(OH)_2$ and NiO nanowalls on various substrates for high-performance nanosensors, Small 11 (2015) 731–739.
[12] J. Zhang, D.W. Zeng, Q. Zhu, J.J. Wu, Q.W. Huang, C.S. Xie, Effect of nickel vacancies on the room-temperature NO_2 sensing properties of mesoporous NiO nanosheets, J. Phys. Chem. C 120 (2016) 3936–3945.
[13] Y.Y. Lv, W.W. Zhan, Y. He, Y.T. Wang, X.J. Kong, Q. Kuang, Z.X. Xie, L.S. Zheng, MOF-templated synthesis of porous Co_3O_4 concave nanocubes with high specific surface area and their gas sensing properties, ACS Appl. Mater. Interf. 6 (2014) 4186–4195.
[14] A. Umar, J.-H. Lee, R. Kumar, O.A. Dossary, A.A. Ibrahim, S. Baskoutas, Development of highly sensitive and selective ethanol sensor based on lance-shaped CuO nanostructures, Mater. Des. 105 (2016) 16–24.
[15] P. Sun, C. Wang, J.Y. Liu, X. Zhou, X.W. Li, X.L. Hu, G.Y. Lu, Hierarchical assembly of α-Fe_2O_3 nanosheets on SnO_2 hollow nanospheres with enhanced ethanol sensing properties, ACS Appl. Mater. Interf. 7 (2015) 19119–19125.
[16] Q.X. Yu, J.H. Zhu, Z.Y. Xu, X.T. Huang, Facile synthesis of α-Fe_2O_3@SnO_2 core–shell heterostructure nanotubes for high performance gas sensors, Sens. Actuat. B: Chem. 213 (2015) 27–34.

[17] S. Park, S. An, Y. Mun, C. Lee, UV-enhanced NO_2 gas sensing properties of SnO_2-core/ZnO-shell nanowire at room temperature, ACS Appl. Mater. Interf. 5 (2013) 4285–4292.
[18] H.-R. Kim, A. Haensch, I.-D. Kim, N. Barsan, U. Weimar, J.-H. Lee, The role of NiO doping in reducing the impact of humidity on the performance of SnO_2-based gas sensors synthesis strategies, and phenomenological and spectroscopic studies, Adv. Funct. Mater. 21 (2011) 4456–4463.
[19] G. Sun, H.L. Chen, Y.W. Li, Z.H. Chen, S.S. Zhang, G.Z. Ma, T.K. Jia, J.L. Cao, H. Bala, X.D. Wang, Z.Y. Zhang, Synthesis and improved gas sensing properties of NiO-decorated SnO_2 microflowers assembled with porous nanorods, Sens. Actuat. B: Chem. 233 (2016) 180–192.
[20] Q. Xu, D.X. Ju, Z.C. Zhang, S. Yuan, J. Zhang, H.Y. Xu, B.Q. Cao, Near room-temperature triethylamine sensor constructed with CuO/ZnO P-N heterostructural nanorods directly on flat electrode, Sens. Actuat. B: Chem. 225 (2016) 16–23.
[21] D. Wen, X.H. Pan, S.S. Chen, C. Chen, Z. Wen, H.H. Zhang, Z.Z. Ye, Honeycomb-like NiO/ZnO heterostructured nanorods: photochemical synthesis, characterization, and enhanced UV detection performance, J. Mater. Chem. C 2 (2014) 4606–4614.
[22] T. Senthil, S. Anandhan, Structure–property relationship of sol–gel electrospun ZnO nanofibers developed for ammonia gas sensing, J. Colloid Interf. Sci. 432 (2014) 285–296.
[23] V.L. Patil, S.A. Vanalakar, P.S. Patil, J.H. Kim, Fabrication of nanostructured ZnO thin films based NO_2 gas sensor via SILAR technique, Sens. Actuat. B: Chem. 239 (2017) 1185–1193.
[24] S.K. Sinha, Synthesis of 1D Sn-doped ZnO hierarchical nanorods with enhanced gas sensing characteristics, Ceram. Int. 41 (2015) 13676–13684.
[25] C.W. Na, H.-S. Woo, I.-D. Kim, J.-H. Lee, Selective detection of NO_2 and C_2H_5OH using a Co_3O_4-decorated ZnO nanowire network sensor, Chem. Commun. 47 (2011) 5148–5150.
[26] F. Chaabouni, M. Abaab, B. Rezig, Metrological characteristics of ZnO oxygen sensor at room temperature, Sens. Actuat. B: Chem. 100 (2004) 200–204.
[27] X. Zhou, W. Feng, C. Wang, X.L. Hu, X.W. Li, P. Sun, K. Shimanoe, N. Yamazoe, G. Y. Lu, Porous ZnO/$ZnCo_2O_4$ hollow spheres: synthesis, characterization, and applications in gas sensing, J. Mater. Chem. A 2 (2014) 17683–17690.
[28] S.R. Wang, X.L. Gao, J.D. Yang, Z.Y. Zhu, H.X. Zhang, Y.S. Wang, Synthesis and gas sensor application of $ZnFe_2O_4$–ZnO composite hollow microspheres, RSC Adv. 4 (2014) 57967–57974.
[29] X.W. Li, P. Sun, T.L. Yang, J. Zhao, Z.Y. Wang, W.N. Wang, Y.P. Liu, G.Y. Lu, Y. Du, Template-free microwave-assisted synthesis of ZnO hollow microspheres and their application in gas sensing, CrystEngComm 15 (2013) 2949–2955.
[30] J.-H. Lee, Gas sensors using hierarchical and hollow oxide nanostructures: overview, Sens. Actuat. B: Chem. 140 (2009) 319–336.
[31] G. Neri, A. Bonavita, G. Micali, G. Rizzo, E. Callone, G. Carturan, Resistive CO gas sensors based on In_2O_3 and $InSnO_x$ nanopowders synthesized via starch-aided sol-gel process for automotive applications, Sens. Actuat. B: Chem. 132 (2008) 224–233.
[32] Y. Shimizu, M. Egashira, Basic aspects and challenges of semiconductor gas sensors, MRS Bull. 24 (1999) 18–24.
[33] K.-I. Choi, H.-J. Kim, Y.C. Kang, J.-H. Lee, Ultraselective and ultrasensitive detection of H_2S in highly humid atmosphere using CuO-loaded SnO_2 hollow spheres for real-time diagnosis of halitosis, Sens. Actuat. B: Chem. 194 (2014) 371–376.
[34] N. Yamazoe, New approaches for improving semiconductor gas sensors, Sens. Actuat. B: Chem. 5 (1991) 7–19.
[35] M. Egashira, Y. Shimizu, Y. Takao, S. Sako, Variation in I-V characteristics of oxide semiconductors induced by oxidizing gases, Sens. Actuat. B: Chem. 35 (1996) 62–67.
[36] T. Weis, R. Lipperheide, U. Wille, S. Brehme, Barrier-controlled carrier transport in microcrystalline semiconducting materials: description within a unified model, J. Appl. Phys. 92 (2002) 1411–1418.
[37] J.C. Dupin, D. Gonbeau, P. Vinatier, A. Levasseur, Systematic XPS studies of metal oxides, hydroxides, and peroxides, Phys. Chem. Chem. Phys. 2 (2000) 1319–1324.
[38] J.-H. Kim, J.-S. Chun, J.W. Kim, W.J. Choi, J.M. Baik, Self-powered, room-temperature electronic nose based on triboelectrification and heterogeneous catalytic reaction, Adv. Funct. Mater. 25 (2015) 7049–7055.
[39] H.-R. Kim, K.-I. Choi, K.-M. Kim, I.-D. Kim, G.Z. Cao, J.-H. Lee, Ultra-fast responding and recovering C_2H_5OH sensors using SnO_2 hollow spheres prepared and activated by Ni templates, Chem. Commun. 46 (2010) 5061–5063.
[40] X.L. Tong, Y. Qin, X.Y. Guo, O. Moutanabbir, X.Y. Ao, E. Pipple, L.B. Zhang, M. Knez, Enhanced catalytic activity for methanol electro-oxidation of uniformly dispersed nickel oxide nanoparticles-carbon nanotube hybrid materials, Small 8 (2012) 3390–3395.
[41] S. Park, G.-J. Sun, C. Jin, H.W. Kim, S. Lee, C. Lee, Synergistic effects of a combination of Cr_2O_3-functionalization and UV-irradiation techniques on the ethanol gas sensing performance of ZnO nanorod gas sensors, ACS Appl. Mater. Interf. 8 (2016) 2805–2811.
[42] C. Liu, B.Q. Wang, T. Liu, P. Sun, Y. Gao, F.M. Liu, G.Y. Lu, Facile synthesis and gas sensing properties of the flower-like NiO-decorated ZnO microstructures, Sens. Actuat. B: Chem. 235 (2016) 294–301.
[43] D.X. Ju, H.Y. Xu, Z.W. Qiu, Zi Chao Zhang, Q. Xu, J. Zhang, J.Q. Wang, B.Q. Cao, Near room temperature, fast-response, and highly sensitive triethylamine sensor assembled with Au-loaded ZnO/SnO_2 core-shell nanorods on flat alumina substrates, ACS Appl. Mater. Interf. 7 (2015) 19163–19171.
[44] S. Salehi, E. Nikan, A.A. Khodadadi, Y. Mortazavi, Highly sensitive carbon nanotubes–SnO_2 nanocomposite sensor for acetone detection in diabetes mellitus breath, Sens. Actuat. B: Chem. 205 (2014) 261–267.
[45] M. Karmaoui, S.G. Lenoardi, M. Latino, D.M. Tobaldi, N. Donato, R.C. Pullar, M.P. Seabra, J.A. Labrincha, G. Neri, Pt-decorated In_2O_3 nanoparticles and their ability as a highly sensitive (<10 ppb) acetone sensor for biomedical applications, Sens. Actuat. B: Chem. 230 (2016) 697–705.
[46] D.R. Miller, S.A. Akbar, P.A. Morris, Nanoscale metal oxide-based heterojunctions for gas sensing: a review, Sens. Actuat. B: Chem. 204 (2014) 250–272.
[47] H.-J. Kim, J.-H. Lee, Highly sensitive and selective gas sensors using p-type oxide semiconductors: overview, Sens. Actuat. B: Chem. 192 (2014) 607–627.
[48] L.L. Wang, Z. Lou, J.N. Deng, R. Zhang, T. Zhang, Ethanol gas detection using a yolk-shell (core-shell) α-Fe_2O_3 nanospheres as sensing material, ACS Appl. Mater. Interf. 7 (2015) 13098–13104.
[49] C.-H. Kwaka, H.-S. Wooa, J.-H. Lee, Selective trimethylamine sensors using Cr_2O_3-decorated SnO_2 nanowires, Sens. Actuat. B: Chem. 204 (2014) 231–238.